Non-destructive procedure to determine residual stresses and white layers in hole making operations

Aitor Madariaga [a,b,*] , Gorka Ortiz-de-Zarate [b] , Pedro J. Arrazola [b]

[a] The University of Manchester, Department of Materials, Oxford Road, Manchester, M13 9PL, UK
[b] Mondragon Unibertsitatea, Faculty of Engineering, Loramendi 4, Arrasate-Mondragón, 20500, Spain

ARTICLE INFO

ABSTRACT

Holes are one of the most critical features of aero-engine components subjected to fatigue loads. Thus, it is essential to ensure a good surface integrity during hole making operations. This work proposes a non-destructive procedure based on X-ray diffraction measurements to determine residual stresses and white layers in holes. Drilling tests were done in Inconel 718 using new and worn tools for different cutting conditions. The results showed that residual stresses can be determined non-destructively with ±150 MPa error. Importantly, Full Width at Half Maximum values showed an unequivocal agreement with the presence of white layer and plastic deformation.

1. Introduction

Nickel alloys possess extraordinary mechanical and corrosion resistance at high temperatures, and they are widely used in aero-engine critical components exposed to high thermomechanical in-service stresses. However, these alloys are difficult to process. A deficient Surface Integrity (SI) generated by machining operations during the last stage of the manufacturing chain can dramatically affect their final performance [1].

Particularly, hole features have one of the highest degree of criticality with reference to fatigue performance of aerospace components [2]. The effect of hole making operations on SI of nickel alloys has been scarcely reported compared to other conventional cutting processes such as turning. Abusive drilling conditions (high cutting speed, use of worn tools or dry conditions) generate a thin white layer and material drag below the surface [3–7]. Severe cutting conditions also increase the hardness near the surface and lead to tensile residual stresses which are higher in the hoop direction than in the axial direction [2,4,6,7]. M'Saoubi et al. [7] demonstrated that nickel alloys with higher Ultimate Tensile Strength are more prone to show higher surface hardness, tensile residual stresses and plastic deformation than reference alloy 718 after abusive drilling.

White layers look white when observed by an optical microscope and they have distinct metallurgical characteristics [7,8]: ultra-fine grain size, increased hardness and strain anisotropy, being more tensile in the

main cutting direction. The presence of white layers can significantly reduce the fatigue strength of nickel alloys and unfortunately, the post-machining shot-peening process is not able to mitigate this reduction [9]. For this reason, reaming and plunge milling operations are carried out after drilling. Careful selection of post-drilling process conditions has shown the ability to remove white layer, tensile surface residual stresses and improve roughness [2,3,6].

Aero-engine components subjected to high temperatures (i.e., turbine discs) and stresses are critical to aircraft safety, and therefore, quality control is highly necessary [10]. These controls are even more necessary to ensure the integrity of critical features such as holes. The above-mentioned studies employed destructive techniques to analyse the SI of holes made in nickel alloys. Evidently, those techniques cannot be used to check the quality of final part in industrial production. Destructive studies allow defining the process window, but do not guarantee that unexpected defects may not occur during production. Recently, non-destructive techniques have been developed to detect white layers in machined surfaces [11,12]. One of these methods consists in performing X-Ray Diffraction (XRD) measurements and analysing the changes of the width of the diffracted peaks (FWHM, Full Width at Half Maximum). They observed that an increase in the value of the FWHM with respect to the reference bulk material can be linked to the generation of a white layer. Authors demonstrated that it is possible to identify and size the thickness of the white layer in milled Ti–6Al–4V and Inconel 718 parts [11], and turned Super CMV and AISI 52100 steels

---

[12]. Nevertheless, other authors found that FWHM of white layers was lower than FWHM of non-damaged surfaces generated by drilling in the superalloy RR1000 [2]. It is also known that FWHM is a good indicator of the level of plastic deformation [2,13], the higher the FWHM value the higher the degree of plastic deformation. In fact, nickel alloys are prone to work-hardening and FWHM can significantly increase with respect to the bulk value [2,14]. Therefore, it is not clear if the increase in FWHM caused by milling in Inconel 718 [11] was as consequence of the properties of the thin white layer or plastic deformation accumulated up to the penetration depth of the X-ray beam.

Additionally, XRD measurements are well established to measure surface residual stresses [15]. Some researchers have measured residual stresses generated by hole making operations in nickel alloys Inconel 718 and RR1000, and stainless steels 316L and 15-5 PH [2,4,6,7,16–18]. However, all those previous studies measured residual stresses using standard XRD methods after cutting the hole. Two main problems arise from this procedure: i) it is destructive and therefore cannot be implemented in industry to verify the surface integrity of real components and ii) surface residual stresses are relaxed/modified as consequence of the cut leading to erroneous results. In fact, Girinon et al. [16] used strain gauges to study the changes in surface stresses when cutting the hole for subsequent residual stress measurements. They concluded that the relaxation was not negligible, and thus, this method cannot accurately determine residual stresses in holes.

This work proposes a non-destructive XRD based approach to determine white layers and residual stresses induced by hole making operations in nickel alloys. To implement the approach, drilling experiments were conducted in Inconel 718 using a variety of conditions that produced different surface conditions. Initially, XRD measurements were done in the holes. Then, the holes were cut, and additional XRD measurements were done to study residual stress relaxation and validate the measurements. Cross sections of the holes were also analysed by optical microscopy and Electron Backscatter Diffraction (EBSD) techniques to characterise white layers and plastic deformation. This allowed a consistent agreement between FWHM of XRD measurements and presence of white layers to be established. Finally, some guidelines are included for implementation in industry.

2. Description of the approach

The $\sin^2\psi$ method is the most common procedure to determine surface residual stresses by XRD technique. To determine the stress σ_Φ in the direction Φ of the surface (Fig. 1a), diffraction patterns are obtained at different tilting angles ψ of the beam relative to the surface normal N and normal to the direction of Φ (Fig. 1b). The angle ψ is the angle between the normal of the surface and bisector of the incident and diffracted beam (cone).

The inter-planar spacing $d_{\Phi\psi}$ of crystallographic planes at an angle ψ

is calculated using Bragg's law defined in eq. (1), where n is an integer, λ is the X-ray wavelength, d is the lattice spacing of crystal planes, and θ is the angle of diffraction. Then each calculated $d_{\Phi\psi}$ is plotted versus $\sin^2\psi$ (Fig. 1c). σ_Φ is given by eq. (2), where E is the Young's modulus, ν is the Poisson's coefficient, and $d_{\Phi0}$ is the crystallographic distance in the unstressed state [19]. The slope of the plot is used to determine $\left(\frac{\partial d_{\Phi\psi}}{\partial\sin^2\psi}\right)$ and $d_{\Phi0}$ is the intercept of the curve at $\sin^2\psi = 0$. The width of the peak is also measured for FWHM use.

$$n\lambda = 2d\sin\theta \qquad \text{(eq.1)}$$

$$\sigma_\Phi = \left(\frac{E}{1+\nu}\right)\frac{1}{d_{\Phi0}}\left(\frac{\partial d_{\Phi\psi}}{\partial\sin^2\psi}\right) \qquad \text{(eq.2)}$$

XRD measurements can be performed on the surface of an uncut hole as shown in the schematic of Fig. 2a. However, there are geometrical constraints that do not enable tilting the beam from one side of the piece to the other (the beam does not reach the surface, or the diffracted beam does not reach the detector, i.e., Det1). Nevertheless, it is possible to define tilting steps from the maximum angle allowed by the XRD equipment to the minimum limited by the upper boundary of the hole, and determine residual stresses. Furthermore, the workpiece can be
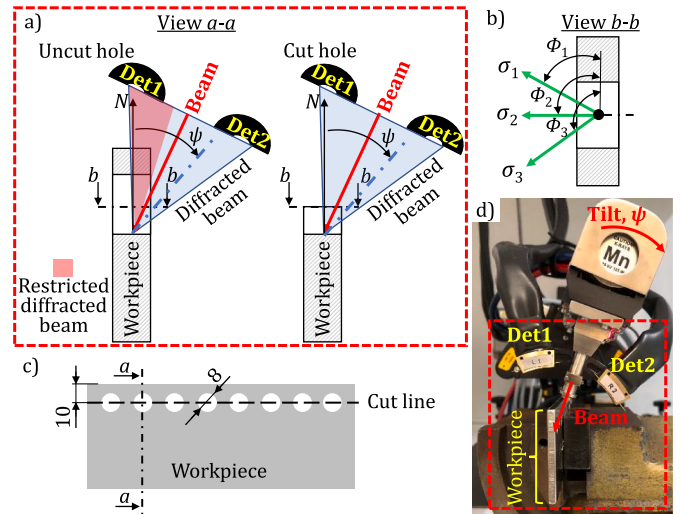

Fig. 2. a) Schematic of the procedure showing the incident and diffracted beam at a tilted angle (ψ) for uncut hole and cut hole and b) top view of the cross section showing residual stress measurement at different directions; c) geometry of the workpiece and d) set-up of XRD measurements used in this work, where the dashed square includes the schematic represented in a). Note: Det1 and Det2 are the detectors.
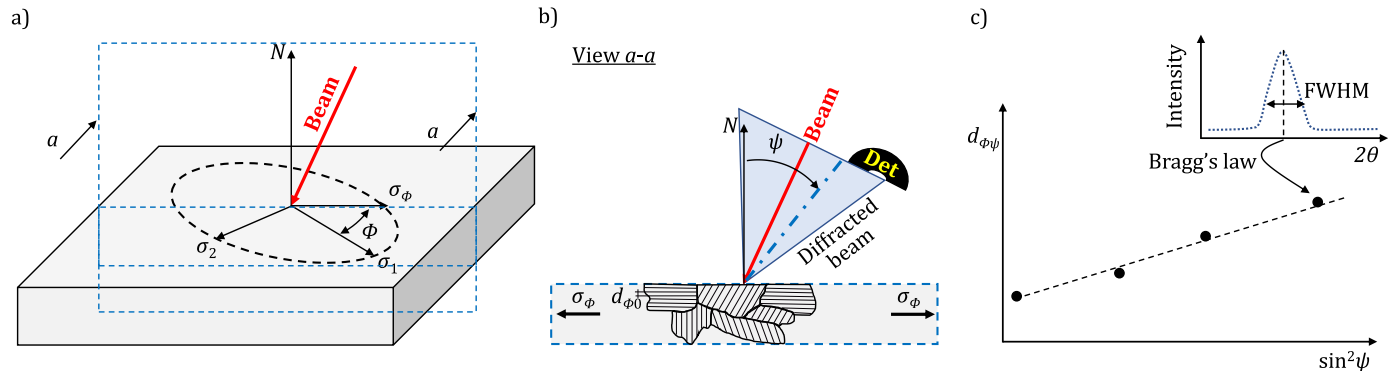

Fig. 1. Schematic of the $\sin^2\psi$ method: a) orientation of the stress σ_Φ in the direction Φ of the surface, b) detailed view of the incident beam and diffracted beam after iteration within the polycrystal and c) example of $d_{\Phi\psi}$ versus $\sin^2\psi$ plot.

rotated (Φ_i) with respect to the surface normal (N) and residual stresses determined in different directions (σ_1, σ_2, σ_3) as shown in the top view of the cross section in Fig. 2b.

3. Materials and experiments

To implement and analyse the feasibility of the approach, drilling tests were done in a 4.25 mm thick Inconel 718 age hardened rolled sheet. Four conditions were used in the tests (changing the cutting speed V_c, feed per tooth f and use of coolant). Each condition was repeated twice, drilling a total of 8 holes of 8 mm diameter (Fig. 2c). The conditions of the tests are summarised in Table 1. Two flutes SUMITOMO solid TiAlN coated carbide tools (MDS080SK) with helix angle of 30° were used. Two tool wear levels were analysed: new and worn tool (initial flank tool wear of $V_b = 0.2$ mm and margin wear of $W_m = 0.4$ mm).

Residual stresses were measured in the holes by XRD using a portable Proto iXRD equipment (Fig. 2d). MnKα radiation was employed (λ = 2.103 Å), with voltage of 25 kV and current of 5 mA to acquire the (311) diffraction peak. A round collimator of 1 mm diameter was used to narrow the irradiated area. Before each measurement, the beam was focused, employing a working distance of 22 mm from the target surface to the collimator. This working distance ensured that the beam was focused during tilting.

Experimental data was analysed by means of PROTO XrdWin software. Diffracted peaks were fitted to a Gaussian function. The diffraction elastic constants used in the measurements were the following: $S_1 = -\nu/E = 1.61\ 10^{-6}$ [MPa^{-1}], ½ $S_2 = 1 + \nu/E = 7.14\ 10^{-6}$ [MPa^{-1}].

The residual stresses were measured at the same points using four procedures as summarised in Table 2. These measurements were done in three directions (Fig. 2b): σ_2 in the axial direction of the hole ($\Phi_2 = 90°$ with respect to the vertical axis), σ_1 and σ_3 oriented $\Phi_1 = 60°$ and $\Phi_3 = 120°$ with respect to the vertical axis. The residual stresses were measured in the uncut hole using the proposed approach: the beam was tilted at four positions from $\psi = 30°$ to 49°, and using one detector (Det2) as shown in the schematic on the left of Fig. 2a. Then, the specimen was cut and XRD measurements were performed (using the configuration shown on the right of Fig. 2a) to analyse the effect of the cut on residual stress relaxation and validate the approach. In the second measurement the beam was tilted at four positions from $\psi = 30°$ to 49°. In some cases, it is possible to access the hole from both sides (for example, in Fig. 2a the beam is on the right side, but it could be used in the left side). Thus, to improve the results, the third measurement used one detector (Det1) at four positions from $\psi = -30°$ to -49° and the second detector (Det2) at four positions from $\psi = 30°$ to 49°. Finally, to validate the proposed approach, the residual stresses were measured using the standard approach: the beam was tilted at nine positions from $\psi = -49°$ to 49° and data was acquired by two detectors (Det1 and Det2).

Subsequently, the microstructural damage of the workpiece was analysed using optical microscopy. The sample preparation procedure began by cutting the samples from the workpiece in the hoop and axial directions. Then, the samples were moulded in resin to be ground, polished, and chemically etched. The microstructural damage was analysed in both directions (hoop and axial). Nevertheless, in the axial direction, any significant microstructural damage was not greater than that observed in the hoop direction. Therefore, the analysis reported in

Table 1
Drilling conditions.

Tool state	V_c (m/min)	f (mm/z)	Coolant	Repetitions
New	15	0.05	Yes	R1, R2
	30	0.1	No	R1, R2
Worn	15	0.05	Yes	R1, R2
	30	0.1	No	R1, R2

Table 2
Summary of the four residual stress measurement procedures.

Procedure	Hole State	Det1	Det2
1st Proposed approach	Uncut	No	$30° \leq \psi \leq 49°$
2nd Measurement	Cut	No	$30° \leq \psi \leq 49°$
3rd Measurement	Cut	$-49° \leq \psi \leq -30°$	$30° \leq \psi \leq 49°$
4th Standard approach	Cut	$-49° \leq \psi \leq 21°$	$-21° \leq \psi \leq 49°$

this work is focused on the hoop direction results. We measured the thickness of the plastically deformed layer and white layer at 10 points of the cross section. The plastically deformed layer was identified by bent grains and/or presence of slip bands. The white layer was considered as the white region with a microstructure completely different to the bulk material.

Finally, the EBSD measurements were carried out using a NOVA NANOSEM 450 at an accelerating voltage of 30 kV. The samples were again prepared following the same methodology as in optical microscopy, replacing the chemical etching with vibropolishing. The step size was 0.4 μm and an area of 120 × 250 μm was measured resulting in approximately 200,000 data points per map. Then, the Kernel Average Misorientation (KAM) was calculated. KAM corresponds with the plastic strain arising from the dislocation motion, which permits the evaluation of the microscale plastic strain in machined surfaces. Finally, the Grain Orientation Spread (GOS) was calculated. This represents the average misorientation angles to the grain mean orientation. Therefore, it only provides a single misorientation for each grain which results in a lower spatial resolution. Nevertheless, it evaluates the local strain of each grain quantitatively.

4. Results and discussion

4.1. Residual stresses

Fig. 3 compares the surface residual stresses (σ_1, σ_2, σ_3) measured in the three directions ($\Phi_1 = 60°$; $\Phi_2 = 90°$; $\Phi_3 = 120°$) using the proposed approach in the initial state (blue solid bars), after cutting the workpiece and using one detector (red stripped bars) and using two detectors detector (green stripped bars), and employing the standard procedure (black dotted bars). Error bars show the error produced when fitting data and applying the sin$^2\psi$ method. The standard method averaged an error of 32 MPa, and a relative error of 16 %. Since the proposed method uses a smaller number of points, an error value of 25 % (with a minimum of 50 MPa) was applied, which is a conservative assumption. It also should be clarified that surface residual stresses varied from the first to the second repetition regardless of the measurement method. These variations could be associated also with the uncertainty of the manufacturing process. The same tool was used in the first and second repetition of each tested condition, and therefore the slight tool wear could have affected the generation of residual stresses. Importantly, the trends of residual stresses are qualitatively consistent in the three directions for the four measurement procedures.

Compressive residual stresses are induced in the axial direction when using coolant, while tensile residual stresses are induced under dry conditions as reported by other researchers [2,6]. When using coolant and new tools, compressive residual stresses are higher in the axial direction than at $\Phi_1 = 60°$ and $\Phi_3 = 120°$. However, when using worn tools and coolant, residual stresses become more compressive at $\Phi_1 = 60°$ and $\Phi_3 = 120°$ than in the axial direction. These results are consistent with the two repetitions, and therefore this confirms that cutting mechanisms changed because of tool wear. The variability of measured tensile residual stresses does not allow us to confirm any change of trend when using new or worn tools under dry conditions.
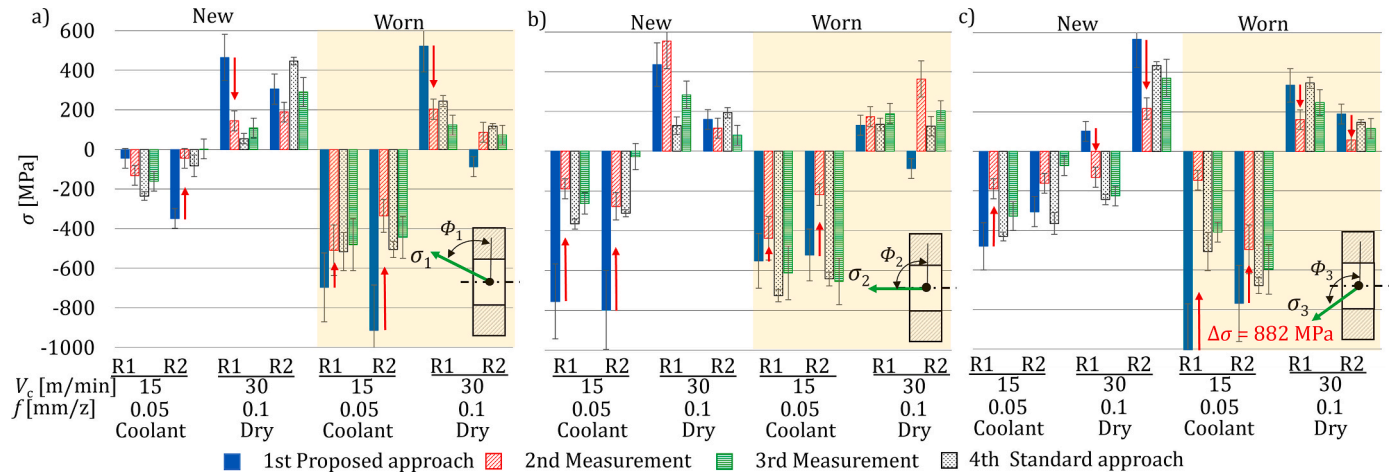
Fig. 3. a) σ_1, b) σ_2 and c) σ_3 surface residual stresses measured before and after cutting the workpiece using the four different procedures.

4.2. Validation of the approach

To validate the proposal, measurements were carried out after cutting the workpiece using the proposed approach with one detector and with two detectors, and following the standard procedure. These results are represented in Fig. 3 by red stripped, green stripped and black dotted lines respectively. Importantly, the three measurements obtained same qualitative trends when changing the drilling conditions. This confirms that even though we use a limited range of angles, we can discern if drilling conditions are severe, leading to more tensile residual stresses or if they induce compressive residual stresses.

To estimate the accuracy of the proposal, the residual stresses measured using one and two detectors were compared to those obtained by the standard full range measurement. Fig. 4a and b show a linear fitting of the residual stresses measured with one detector and two detectors respectively. The border lines are limiting a deviation of ±150 MPa with respect to the linear fitting.
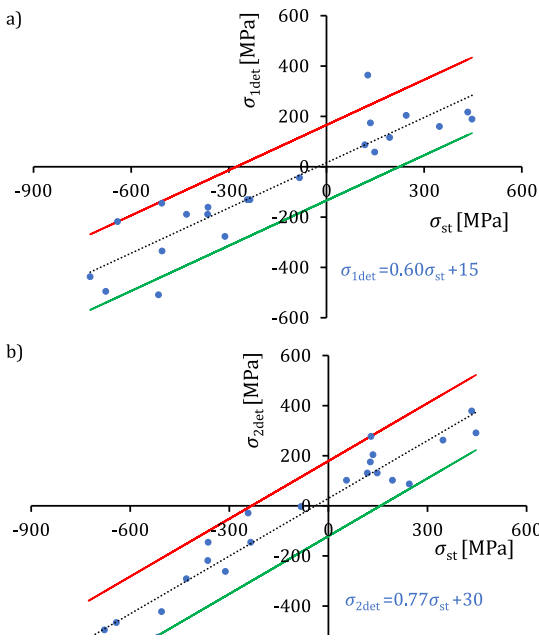

Fig. 4. a) Residual stresses measured with one detector (σ_{1det}) and b) two detectors (σ_{2det}) vs residual stresses measured with the standard procedure (σ_{st}), including fitted linear regressions.

The proposed procedure underestimates the real residual stresses by 40 % (0.6, coefficient of the linear regression showed in Fig. 4a) and most of the result would be predicted with an error of ±150 MPa. Note that the scatter of results is higher in the tensile regime. The results are improved when using two detectors. Residual stresses are underestimated only by 23 % (0.77, coefficient of the linear regression shown in Fig. 4b), and almost all points are predicted with an error of ±150 MPa.

Fig. 5 shows two examples of the d_ψ plot versus $\sin^2\psi$ obtained using the standard measurement, the proposed approach with two detectors and one detector. A linear fitting was applied to compare the three methods, despite being evident that severe drilling conditions led to higher shear stresses and an elliptical fitting would have been better under such conditions (Fig. 5b). The use of two detectors enables the acquisition of more data, and thus a better fitting in the $\sin^2\psi$ technique. The second reason is the effect of shear stresses on acquisition data and subsequent fitting. Machining induces shear stresses in the surface layer, which increase under severe cutting conditions. The higher the shear stress, the d_ψ plot versus $\sin^2\psi$ of one detector with respect to the other diverges more. Thus, they have different slope and each one will lead to different residual stress value according to eq. (2) when fitting independently. Consequently, under high shear stresses, the use of one detector can lead to higher errors.

4.3. Relaxation of residual stresses

The residual stresses measured in the holes before (blue solid bars) and after the cut (red stripped bars) using the proposed method with one detector are compared in Fig. 3. Both measurements obtained similar quantitative trends when changing drilling conditions. However, the relaxation caused by the cut is evident. In most cases it exceeds the error of ±150 MPa reported in the preceding discussion. These conditions are highlighted with red arrows in Fig. 3. Compressive residual stresses induced when using coolant were lower after the cut. The relaxation of residual stresses was more evident at $\Phi_1 = 60°$ and $\Phi_3 = 120°$ orientation than in the axial direction of the hole ($\Phi_2 = 90°$). From the 24 measurements, 19 showed relaxation, ranging from 110 MPa to 882 MPa. This means an average of 43 % relaxation with respect to the initial residual stress condition. The relaxation of residual depends on the initial state prior to cutting the hole. The different drilling conditions led to different initial residual stress fields. The highest relaxation was observed in the surfaces with higher initial residual stresses.

Previous studies on residual stresses generated by hole making operations did the measurements after having the hole cut into two. Kwong et al. suggested that the layer affected by the machining conditions was
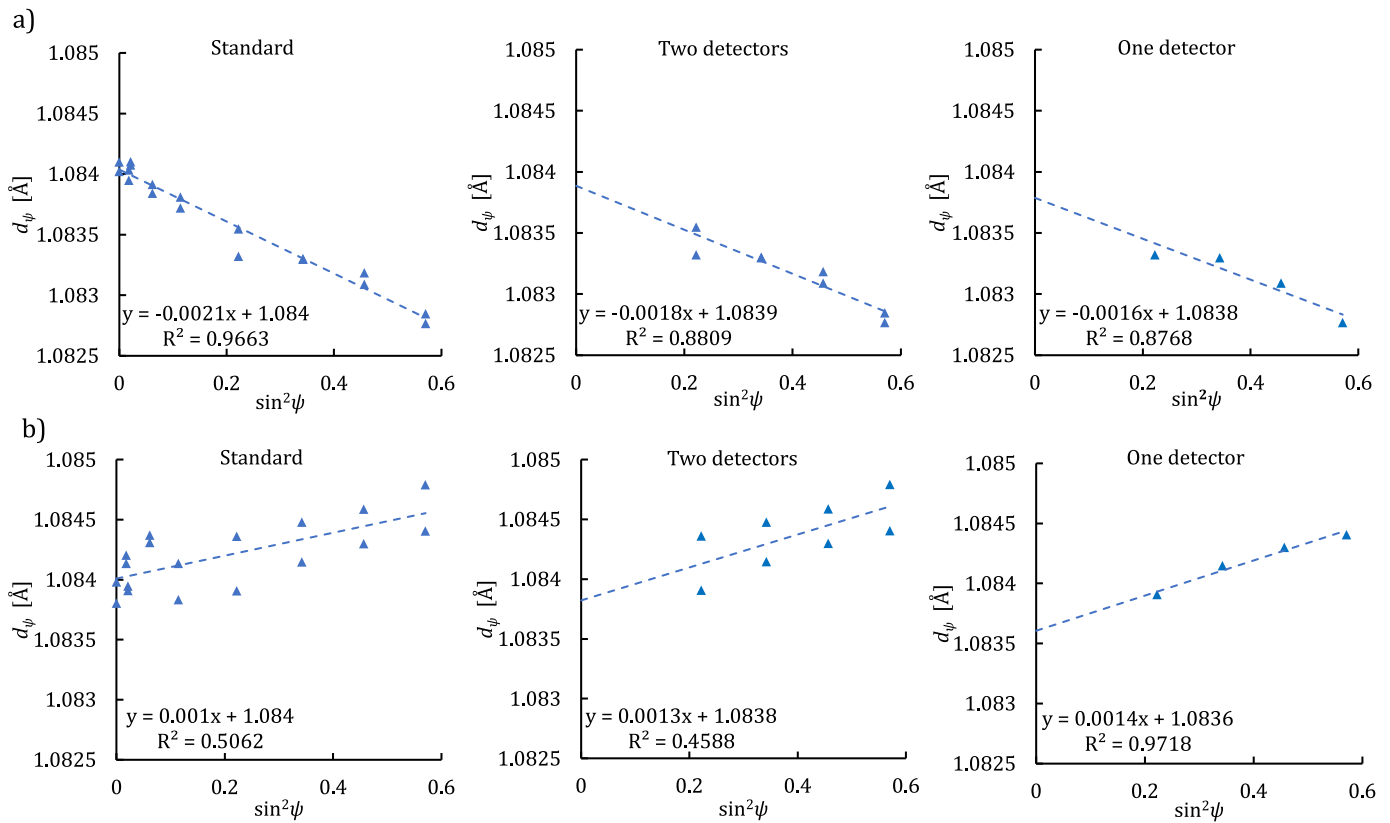
a)

b)

Fig. 5. Comparative of d_ψ plot versus $\sin^2\psi$ obtained with different methods in the $\Phi_2 = 90°$ direction: a) $V_c = 15$ m/min, $f = 0.05$ mm/z, coolant, new tool, 2nd repetition; b) $V_c = 30$ m/min, $f = 0.1$ mm/z, dry, worn tool, 1st repetition.

much thinner than the workpiece and therefore the relaxation is negligible [4], but they did not study rigorously the relaxation caused by the cutting. By contrast, Girinon and co-workers used strain gauges to quantify the relaxation of residual stresses during the cutting of the hole and concluded that it is not negligible [16]. The results of the present work also confirm that residual stress relaxation is not negligible.

4.4. Plastic deformation and white layer

Fig. 6 shows the dependence of FWHM (left scale) and plastic deformation and white layer depth (right scale) on the drilling conditions. The FWHM shows the average value of the FWHM measured in all the diffraction peaks analysed in the three directions ($\Phi_1 = 60°$, $\Phi_2 = 90°$ and $\Phi_3 = 120°$) for each surface condition. The plastic deformation and white layer thickness show the average value of the 10 measurements done in the cross section of each tested hole, and the error bars

Fig. 6. FWHM of drilled holes and thickness of plastic deformation and white layers.

represent the standard deviation. The results fall into two main groups. With coolant, the plastic deformation depth ranges from 18 to 60 μm and there is no presence of white layers when using either new or worn tools (4 sets of measurement). For those conditions FWHM is from 4.8 to 5.1°. Under dry conditions, the white layer depth is 20–30 μm and plastic deformation depth is 110–130 μm (3 sets of measurement). Then FWHM is in the range 3.3–3.8°. The exception is the 1st repetition of dry conditions with new tools, which did not induce a white layer and deep plastic deformation, and it showed a higher value of FWHM. A new drill bit was used to drill the first hole and the same drill bit was employed in the second repetition. The slight wear generated during the first repetition could have increased the temperatures and cutting forces in the second repetition, and consequently, led to tensile residual stresses in all directions, a thicker deformed layer and presence of white layer.

The microstructure of the surface of the holes was observed initially using optical microscopy, and then in more detail by KAM and GOS maps obtained by the EBSD analysis. KAM value increases when dislocation density increases. Since plastic deformation leads to dislocations, KAM is a good indicator of the severe plastic deformation. GOS provides the average misorientation angles to the grain mean orientation, and thus it also increases with plastic deformation. Both parameters are used to analyse plastic deformations caused by machining. Some examples of these observations are summarised in Fig. 7. All the surfaces show material drag near the surface and sometimes evidence of slip bands as consequence of the strain hardening. The depth of the plastic deformation (maximum depth between material drag and strain hardening) varies depending on drilling conditions. It significantly increases when using worn tools (see Fig. 6). More critically, white layers with a thickness from 20 to 30 μm are observed in the surfaces with the lowest FWHM, below 3.8°. Moreover, tensile stresses were also measured in all directions of those surfaces (see Fig. 3).

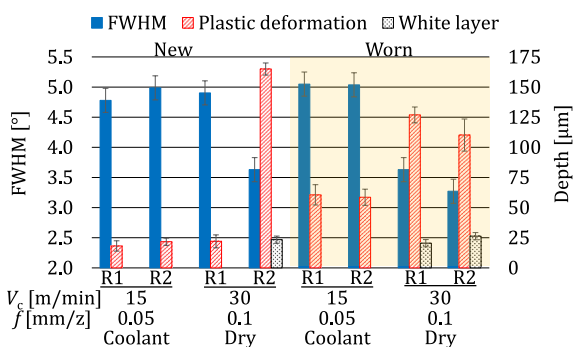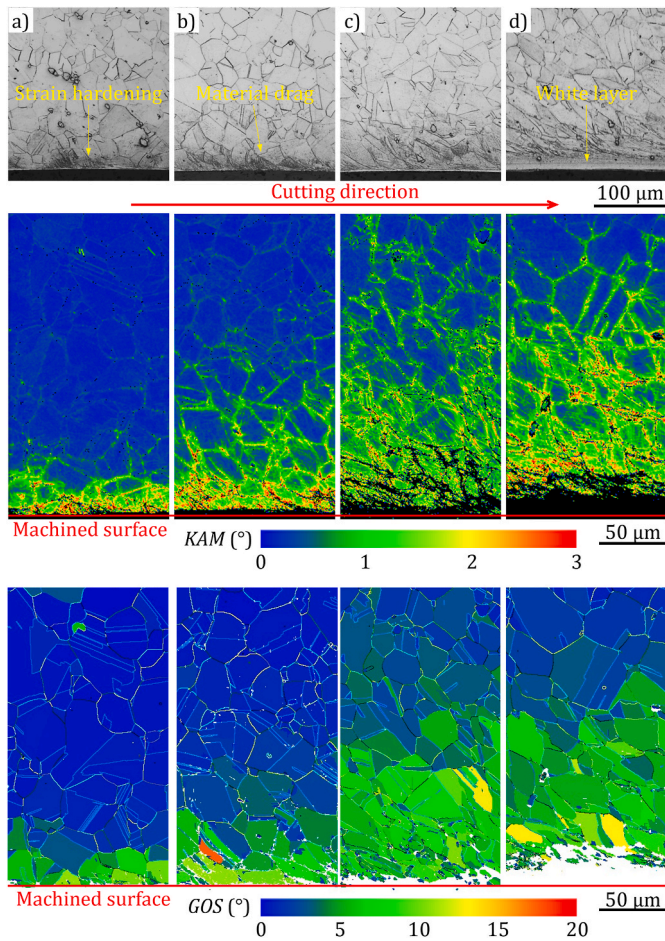For the XRD parameters used in this project the FWHM of the bulk

Fig. 7. Examples of microstructure defects observed by optical microscope and EBSD analysis (KAM and GOS maps): a) $V_c = 15$ m/min, $f = 0.05$ mm/z, coolant, new tool; b) $V_c = 30$ m/min, $f = 0.1$ mm/z, dry, new tool; c) $V_c = 30$ m/min, $f = 0.1$ mm/z, dry, new tool; d) $V_c = 30$ m/min, f = 0.1 mm/z, dry, worn tool (all are the 1st repetition).

material is $\approx 2°$. Thus, there is a notable increase of the FWHM compared to the bulk material. In general, the highest values of FWHM were obtained when using coolant. By contrast, drilling under dry conditions with worn tools led to a significant decrease of the FWHM. The second repetition using $V_c = 30$ m/min, $f = 0.1$ mm/z under dry conditions with a new tool also decreased the FWHM. In fact, under those severe conditions high thermomechanical loads are generated and are likely to induce white layers in holes as observed by [3–7]. White layers were only present when the value of FWHM showed a significant drop with respect to gentle drilling conditions (see Fig. 6). This agrees with the results found by Kwong et al. [2] when drilling the alloy RR1000.

The penetration depth of MnKα radiation in nickel superalloys ranges from 12 to 22 μm for the X-ray incident beam angles used in this work [4,11]. Thus, the decrease in FWHM is associated with the signal acquired in the white layer. The main factors affecting the FWHM are the background signal, the grain size and the plastic deformation [2]. The set-up and parameters used in the XRD measurements were not modified throughout the study and therefore the background effect can be excluded when comparing the FWHM values induced by different drilling tests. It is generally reported that a reduction of grain size increases the FWHM [20]. Drilling induced white layers in nickel alloys are formed by nanocrystal ranging from 20 to 100 nm [7], and therefore much smaller than the grain size of the raw material. This would imply an increase in the FWHM when generating white layers, but the results

depicted in Fig. 6 clearly show that it decreases compared to machined surface without white layers. The severe plastic deformation induced by the drilling process also increases the FWHM (Fig. 6), and it was also reported when drilling alloy RR1000 [2]. However, during severe drilling conditions high temperatures are reached. Cuesta et al. [21] estimated a temperature increase of ≈ 1000 °C when drilling Inconel 718 under dry conditions compared to ≈ 300 °C when using coolant. As consequence of those high temperatures plastic strains partially relax within the white layer, leading to a reduction of FWHM [2].

4.5. General guidelines

The approach introduced in this paper could be used in industry to assess non-destructively surface residual stresses and severe damage (generation of white layers and plastic deformation) in holes for different materials. Although the approach has been validated in holes made by drilling, it could be applied to analyse residual stresses induced by other hole making operations such as reaming or milling. For its implementation, firstly a calibration procedure should be conducted, comparing results from uncut hole measured with the proposed approach, and cut hole measured by both the proposed approach and standard XRD procedure. To increase the accuracy of the residual stress measurements, the range of tilting angle ψ should be set at the maximum, as well as the number of tilts, which is limited by the geometric constraints. The working distance also must be correctly defined, and it is mandatory to ensure that the beam is focused on the measurement point during ψ tilting. This will help to establish the regression models (i.e, as shown in Fig. 4) to quantify surface residual stresses and threshold values of FWHM to identify presence of white layers.

5. Conclusions

The proposed method can be used to non-destructively analyse surface residual stresses and detect the presence of white layers induced by hole making operations in nickel alloys. The following key findings are highlighted.

- Residual stresses are relaxed when cutting the hole. This is more evident when the magnitude of residual stresses is higher. In this work the relaxation ranges from 110 to 882 MPa, with an average relaxation of 43 % with respect to the initial residual stresses.
- The residual stresses are underestimated by 40 %, and 75 % of the results are predicted with an error lower than ± 150 MPa when only one detector is used. If the hole can be accessed from both sides and two detectors are used, the results are improved, underestimated by 23 % but almost all are below ± 150 MPa error.
- The value of FWHM decreases under dry conditions as a consequence of the great amount of heat transfer into the workpiece causing relaxation of plastic strains near the surface. A high reduction of the FWHM value confirms the presence of thick white layers (around 20 μm or more). Furthermore, these white layers are accompanied with tensile surface residual stresses. Additionally, an increase of the FWHM shows a good agreement with the increase of plastically deformed layer when there are no white layers.

CRediT authorship contribution statement

Aitor Madariaga: Conceptualization, Formal analysis, Investigation, Methodology, Writing – original draft, Writing – review & editing. **Gorka Ortiz-de-Zarate:** Conceptualization, Investigation, Methodology, Resources, Writing – review & editing. **Pedro J. Arrazola:** Funding acquisition, Methodology, Resources, Supervision, Validation, Writing – review & editing.

Declaration of competing interest

The authors declare that they have no known competing financial interests or personal relationships that could have appeared to influence the work reported in this paper.

Acknowledgements

Data availability

Data will be made available on request.

References

[1] Jawahir IS, Brinksmeier E, M'Saoubi R, Aspinwall DK, Outeiro JC, Meyer D, Umbrello D, Jayal AD. Surface integrity in material removal processes: recent advances. CIRP Annals 2011;60/2:603–26. https://doi.org/10.1016/j.cirp.2011.05.002.

[2] Kwong J, Axinte DA, Withers PJ. The sensitivity of Ni-based superalloy to hole making operations: influence of process parameters on subsurface damage and residual stress. J Mater Process Technol 2009;209:3968–77. https://doi.org/10.1016/j.jmatprotec.2008.09.014.

[3] Sharman ARC, Amarasinghe A, Ridgway K. Tool life and surface integrity aspects when drilling and hole making in Inconel 718. J Mater Process Technol 2008;200 (1–3):24–432. https://doi.org/10.1016/j.jmatprotec.2007.08.080.

[4] Kwong J, Axinte DA, Withers PJ, Hardy MC. Minor cutting edge–workpiece interactions in drilling of an advanced nickel-based superalloy. Int J Mach Tool Manufact 2009;49(7–8):645–58. https://doi.org/10.1016/j.ijmachtools.2009.01.012.

[5] Soo SL, Hood R, Aspinwall DK, Voice WE, Sage C. Machinability and surface integrity of RR1000 nickel based superalloy. CIRP annals 2011;60/1:89–92. https://doi.org/10.1016/j.cirp.2011.03.094.

[6] Herbert CRJ, Kwong J, Kong MC, Axinte DA, Hardy MC, Withers PJ. An evaluation of the evolution of workpiece surface integrity in hole making operations for a nickel-based superalloy. J Mater Process Technol 2012;212/8:1723–30. https://doi.org/10.1016/j.jmatprotec.2012.03.014.

[7] M'Saoubi R, Axinte D, Herbert C, Hardy M, Salmon P. Surface integrity of nickel-based alloys subjected to severe plastic deformation by abusive drilling. CIRP Annals 2014;63/1:61–4. https://doi.org/10.1016/j.cirp.2014.03.067.

[8] Marçal LAB, Dierks H, Bushlya V, Lazar I, Dzhigaev D, Ren Z, Rysov R, Björling A, Sprung M, Mikkelsen A, Lenrick F, M'Saoubi R, Wallentin J. Spatially resolved structural and chemical properties of the white layer in machined Inconel 718 super alloy. Mater Des 2014;239:112789. https://doi.org/10.1016/j.matdes.2024.112789.

[9] Herbert C, Axinte DA, Hardy M, Withers P. Influence of surface anomalies following hole making operations on the fatigue performance for a nickel-based superalloy. J Manuf Sci Eng 2014;136/5:051016. https://doi.org/10.1115/1.4027619.

[10] M'Saoubi R, Axinte D, Soo SL, Nobel C, Attia H, Kappmeyer G, Engin S, Sim WM. High performance cutting of advanced aerospace alloys and composite materials. CIRP Annals 2015;64/2:557–80. https://doi.org/10.1016/j.cirp.2015.05.002.

[11] Brown M, Pieris D, Wright D, Crawforth P, M'Saoubi R, McGourlay J, Mantle A, Patel R, Smith RJ, Ghadbeigi H. Non-destructive detection of machining-induced white layers through grain size and crystallographic texture-sensitive methods. Mater Des 2021;200:109472. https://doi.org/10.1016/j.matdes.2021.109472.

[12] Brown M, Crawforth P, Curtis D. Rapid non-destructive sizing of microstructural surface integrity features using x-ray diffraction. NDT Int 2022:102682. https://doi.org/10.1016/j.ndteint.2022.102682.

[13] Naskar A, Paul S. Non-destructive measurement of grinding-induced deformation-depth using grazing incidence X-ray diffraction technique. NDT Int 2022;126:102592. https://doi.org/10.1016/j.ndteint.2021.102592.

[14] Madariaga A, Esnaola JA, Fernandez E, Arrazola PJ, Garay A, Morel F. Analysis of residual stress and work-hardened profiles on Inconel 718 when face turning with large-nose radius tools. Int J Adv Manuf Technol 2014;71:1587–98. https://doi.org/10.1007/s00170-013-5585-6.

[15] Velicheti D, Nagy PB, Hassan W. Residual stress and cold work assessment in shot-peened IN718 using a dual-mode electromagnetic technique. NDT Int 2021;121:102463. https://doi.org/10.1016/j.ndteint.2021.102463.

[16] Girinon M, Valiorgue F, Rech J, Feulvarch E. Development of a procedure to characterize residual stresses induced by drilling. Procedia CIRP 2016;45:79–82. https://doi.org/10.1016/j.procir.2016.02.074.

[17] Girinon M, Dumont F, Valiorgue F, Rech J, Feulvarch E, Lefebvre F, Karaouni H, Jourden E. Influence of lubrication modes on residual stresses generation in drilling of 316L, 15-5PH and Inconel 718 alloys. Procedia CIRP 2018;7141–6. https://doi.org/10.1016/j.procir.2018.05.020.

[18] Leveille T, Granier C, Valiorgue F, Pascal H, Rech J, Van-Robaeys A, Lefebvre F, Kolmacka J, Dorlin T. Characterization of residual stresses induced by a multistep hole making sequence. Procedia CIRP 2021;102:477–81. https://doi.org/10.1016/j.procir.2021.09.081.

[19] Prevey PS. X-ray diffraction residual stress techniques, vol. 10. ASM International, ASM Handbook; 1986. p. 380–92. https://doi.org/10.31399/asm.hb.v10.a0001761.

[20] Unal O, Varol R. Surface severe plastic deformation of AISI 304 via conventional shot peening, severe shot peening and repeening. Appl Surf Sci 2015;351:289–95. https://doi.org/10.1016/j.apsusc.2015.05.093.

[21] Cuesta M, Aristimuño P, Garay A, Arrazola PJ. Heat transferred to the workpiece based on temperature measurements by IR technique in dry and lubricated drilling of Inconel 718. Appl Therm Eng 2015;104:309–18. https://doi.org/10.1016/j.applthermaleng.2016.05.040.